Estimating the global reduction in transmission and rise in detection capacity of the novel coronavirus SARS-CoV-2 in early 2020

Antoine Belloir[1]

François Blanquart[2,3]

1. Ecole Polytechnique, Route de Saclay, 91120 Palaiseau, France.

2. Centre for Interdisciplinary Research in Biology (CIRB), Collège de France, CNRS, INSERM, PSL Research University, Paris, France.

3. Infection Antimicrobials Modelling Evolution, UMR 1137, INSERM, Université de Paris, Paris, France

Abstract

To better control the SARS-CoV-2 pandemic, it is essential to quantify the impact of control measures and the fraction of infected individuals that are detected. To this end we developed a deterministic transmission model based on the renewal equation and fitted the model to daily case and death data in the first few months of 2020 in 79 countries and states, representing more than 4 billions individuals. Based on a region-specific infected fatality ratio, we inferred the time-varying probability of case detection and the time-varying decline in transmissiblity. The model was validated by the good correlation between the predicted total number of infected and that found in serosurveys; and most importantly by the strong correlation between the inferred probability of detection and the number of daily tests per inhabitant, with 50% detection achieved with 0.003 daily tests per inhabitants. Most of the decline in transmission was explained by the reductions in transmissibility (social distancing), which avoided 10^7 deaths in the regions studied over the first four months of 2020. In contrast, symptom-based testing and isolation was not an efficient way to control the spread of the disease, as a large part of transmission happens before symptoms and only a small fraction of infected individuals was typically detected. We developed a phenomenological model to link the number of daily tests with the probability of detection and verified the prediction that increasing test capacity increases the probability of detection less than proportionally. Together these results suggest that little control can be achieved by symptom-based testing and isolation alone.

Introduction

The coronavirus SARS-CoV-2 originated in November-December 2019 (1), appeared as a cluster of cases of pneumonia of unknown etiology in the Wuhan province in China in December 2019-January 2020, and subsequently spread in Asia, Europe, North America, and the rest of the world in 2020. The rapid doubling time associated with the basic reproductive number R_0 at 2-3 (2–4), together with the fact that an estimated ~50% of transmission is presymptomatic (5,6) make it difficult to control. A substantial proportion of infected individuals need to be hospitalised: 1 to 18% with increasing age in China, 4% overall in France (7–9). The infected fatality ratio (IFR) is around 1%, and much higher in the elderly (7–10).

By early March 2020, many regions of the world had imposed strong social distancing measures to reduce transmission and contain the spread of SARS-CoV-2. These social distancing measures were varied and included school closure, business closure, partial or full lockdowns, stay-at-home order, the prohibition of gatherings, curfews, etc. These measures resulted in the stabilisation or the inversion of the epidemic curve in many countries (11). This was accompanied by an increase in the capacity to PCR-test potentially infected individuals.

To improve the control of the epidemic, it is necessary to understand the transmission dynamics during the period of unrestricted growth in the first few months of 2020, and the impact of the subsequent reduction in transmission owing to (i) the depletion of susceptible individuals , (ii) the social distancing measures implemented, (iii) tests and isolation of cases. We develop a dynamical epidemiological model that describes the transmission dynamics with a discrete-time renewal equation. Thanks to published estimates of the IFR, our model predicts the daily number of all cases and the fraction of detected cases, and the daily number of deaths over the course of the epidemic and can thus be readily fit to data from 79 countries, states and provinces. Within each of these regions, we infer the time-varying probability of detection; the time-varying transmissibility; and we deduce the impact of detection and case isolation on transmission dynamics. The model is validated by the strong correlation between the predicted attack rate and that found in serological surveys. Finally, we show that the capacity to detect SARS-CoV-2 infections is strongly related to the number of tests performed per inhabitant, develop a novel model that relate the number of tests to the probability of detection and verify the model predictions. These results will serve to better understand and control transmission dynamics.

Results:

We model the dynamics of SARS-CoV-2 transmission for 79 geographical zones (countries, USA states, Canadian provinces and the Hubei province in China; hereafter "regions") with a discrete-time renewal equation that describes how individuals are infected each day by transmission from previously infected individuals (Methods). Our model is akin to an existing model that predicts the daily number of deaths (11). The adapted renewal equation we use predicts in a deterministic way the daily numbers of infected, cases recorded, and deaths, given temporal profiles of transmissibility and case detection.

Infected individuals may die with a constant probability called the infected fatality ratio (IFR). We fix both the IFR and the distribution of time to death to values previously estimated from data from mainland China (8). The inference of the number of infected and hence the probability of detection crucially relies on the IFR, which links the daily deaths with the past number of infected individuals . The IFR is difficult to estimate because case detection is biased towards more severe cases. Early estimates relied on settings where tests were exhaustive such as repatriation flights or the Diamond Princess cruise boat (7,8,12). We use one of the published estimates of age-dependent IFR ((12); similar to other estimates, Supplementary Fig. 1) to compute a region-specific IFR that takes into account the regional age distribution. This region-specific IFR ranges from 0.3-0.4% (Bangladesh, Egypt, Pakistan, Philippines, South Africa) to 1.2%-1.4% (Germany, Italy, Portugal, Spain), and is typically around 1% in the regions examined (median 0.94%). The IFR and the distribution of the time from infection to death allows us to project back in time the number of infected individuals.

We fit jointly the number of cases and deaths. This strategy has two advantages. While the number of deaths may be small, the number of cases is typically much larger and less subject to stochastic fluctuations. Furthermore, cases give an early signal of potential changes in transmissibility, as infected individuals may be detected as soon as symptoms occur, about a week after infection, while death occurs much later, about four weeks after infection on average. The number of recorded cases, however, depends on the intensity of testing and the testing strategy. We account for changes in intensity of testing by modelling sand inferring a time-varying probability of case detection. We can thus interpret the number of cases recorded jointly with the number of deaths. Case detection is assumed to happen typically a few days after symptom onset, as inferred from (13), and to be followed by perfect isolation. Isolation reduces the pool of infected individuals who contribute to transmission (Methods).

From the renewal equation framework predicting the daily number of cases and deaths, we infer the time-varying transmission rate and the time-varying detection probability in the 79 studied regions. The chosen regions are those where the daily death incidence had reached 10 deaths at least once as of 23rd April 2020 according to the John Hopkins Coronavirus Resource Center database. We fit the model by maximum likelihood to the case and death count data assuming the data points each day are drawn in a negative binomial distribution with mean given by the model prediction, and with an inferred dispersion parameter.

We validate our projections by comparing the inferred total attack rates—the proportion of individuals in the population that have ever been infected at a given date—with the number of infected individuals in nine regions where the number of infected at a certain time is known by systematic survey on a representative sample. The attack rate is given by the result of seroprevalence surveys, where a seropositive individuals is assumed to have been infected no later than 13 days in the past, corresponding to the median time to seroconversion (14). Note that in one case (Austria) we use results from a systematic PCR test survey. In that one case a positive individual is assumed to have been infected in the interval from 20 to 4 days ago (15) The attack rate predicted by our analysis was generally close to that in the data (Fig. 1), with no systematic bias. Countries above the identity line have more positive individuals in reality than predicted by the model. For these countries the true IFR is lower than the one assumed: given the realised number of deaths, the country actually had more infected individuals than what the model predicts. On the contrary, countries below the identity line have a higher IFR than the one assumed. Deviations of the true IFR from that assumed in the model bias the estimated absolute value of the detection probability, but not the temporal trends in the detection probability.

To study the change in transmission following social distancing measures, one could infer the effects of different types of measures such as business, school, bar and restaurant closures, banning large gatherings, lockdowns, etc. However, these measures and their implementations are very varied across regions and multiple measures are often implemented simultaneously and may be accompanied by undocumented behavioural changes, complicating the inference of effects of individual measures (11). Instead, we estimate a region-specific reduction in transmissibility. We test two functional forms for the decline in transmissibility: (i) a sharp reduction in transmissibility at th date of the strongest social distancing measure. This was in most cases a national (or state-wise) lockdown (65 regions), regional lockdowns (5 regions: Algeria, Brazil, Indonesia, Oklahoma, Russia) or a variety of distancing measures with no strict

lockdown (9 regions: British Columbia, Canada, Chile, Dominican Republic, Egypt, Iran, Ontario, Sweden, Turkey); (ii) a smooth sigmoid reduction in transmissibility. When comparing the fit of the two models with the Akaike Information Criterion (AIC), the smooth reduction in transmissibility fitted that data better (an AIC difference greater than 4) in 50 regions out of 79. In these cases the reduction in transmissibility predated the date of the strongest social distancing measure by 5 to 20 days (Supplementary Fig. 3). In the 29 other regions, both functional forms were similar (Supplementary Fig. 2).

In most regions, we find a strong reduction in transmissibility accompanied by an increase in detection capacity. The basic reproduction number $R_{0,t}$ decreased from 3.7 on average across countries at the first date when 5 daily cases were reached, to 0.98 as of 8th of May (Fig. 2B). There is substantial variation in the inferred initial transmissibility across regions. The mean probability of detection increased from 4% to 29% over the same period (Fig. 2C). The transmissibility remained above 1 (the threshold above which the epidemic expands in the absence of other measures) in several regions as of 8th May, including Minnesotta, Brazil, Mexico, Pakistan, South Africa (Fig. 3A). The type of social distancing measure (national lockdown, regional lockdown, distancing) did not affect the final transmissibility (linear model for the final transmissibility as a function of the distancing measure; p= 0.46). The probability of detection as of 8th May was below 50% for 67 out of 79 regions (Fig. 2B). The model predicted an attack rate of infection across regions of 0.1% (India) to 15% (New Jersey, USA).

<u>Factors contributing to the reduction to transmission:</u> The effective reproduction number $R^E_{t_{final}}$ on the 8th of May (t_{final}), including the impacts of detection and isolation and immunity may be written as the product of the initial basic reproduction $R_{0,t_{init}}$ number times three factors that all reduce transmission:

$$R^E_{t_{final}} = R_{0,t_{init}} \underbrace{\left(1-\mathcal{A}_{t_{final}}\right)}_{\text{(i) immunity}} \underbrace{\left(1-\mathcal{B}_{t_{final}}\right)}_{\text{(ii) reduced transmissibility}} \underbrace{\left(1-\mathcal{C}_{t_{final}}\right)}_{\text{(iii) detection and isolation}}$$

with $\mathcal{A}_{t_{final}} = I^{tot}_{t_{final}}/S_0$, $\mathcal{B}_{t_{final}} = 1 - R_{0,t_{final}}/R_{0,t_{init}}$, and $\mathcal{C}_{t_{final}} \propto c_{t_{final}}$ (Material and Methods). The reduction in overall transmission depends on (i) the depletion of the pool of susceptibles, (ii) reduced transmissibility impacting the basic reproduction number $R_{0,t}$, (iii) testing and case isolation. We found that the factor contributing most to reduced transmission is the reduced transmissibility (Fig. 4B).

155 The reduction in transmission owing to population immunity depends on the total number of
156 individuals ever infected $I_{t_{final}}^{tot}$ (the attack rate) over the initial number of susceptible
157 individuals S_0, assumed to be the total population size of the region. The attack rate was smaller
158 than 2% in 47 regions out of 79. The reduction in the number of susceptible individuals that
159 could lead to herd immunity is thus very small in most regions, assuming that all individuals
160 are initially susceptible. The second factor is estimated from the inferred sigmoid curve for
161 $R_{0,t}$. The third factor is estimated assuming that case detection is followed by strict isolation,
162 such that a detected case stops transmitting and the generation time is effectively truncated
163 (Fig. 4A). This assumption is compatible with evidence that generation times are shortened by
164 case isolation (16,17). With our set of parameters, the reduction owing to detection and
165 isolation is approximately $\mathcal{C}_{t_{final}} = 0.46\, c_{t_{final}}$. That is, on average detection and isolation
166 only prevents 46% of transmission of a detected individual. The resulting reduction in
167 transmission caused by detection and isolation is typically small (even under the conservative
168 assumption that all detected individuals are perfectly isolated) because a small fraction of
169 infected individuals is detected, and because individuals are detected a few days after
170 symptoms when about half of the transmission already occurred (5,6).

171 To estimate the number of deaths averted by social distancing from the beginning of the
172 epidemic to May 8th, we simulated the epidemic in the absence of social distancing measures,
173 i.e. when transmissibility remains constant at its inferred initial value. The difference between
174 the simulated number of deaths and the true reported number of deaths is the number of deaths
175 averted. The reductions in transmissibility fom the beginning of the epidemic to May 8th
176 avoided in total across these regions 9.8×10^6 deaths, and of the order of 10^4 to 10^6 deaths per
177 country. Brazil, Mexico and large European countries (France, Germany, Italy, Spain, United
178 Kingdom) avoided 5 to 8×10^5 deaths. A previous study of 11 European countries reported
179 figures similar to ours (4.7 to 7.2×10^5 deaths avoided in the five aforementioneds countries
180 (11)).

181 <u>Mobility as a correlate of transmission:</u> the inferred time-varying transmissibility correlated
182 with indicators of mobility. This has been evidenced in other studies in the USA (18,19).
183 Precisely, we use the Google COVID-19 Community Mobility Reports which record the
184 presence of individuals each day at six types of location: grocery & pharmacy, parks, transit
185 stations, retail & recreation, residential, and workplaces, for most regions studied here (with
186 the exception of Algeria, the Hubei province in China, Iran, Morocco, Russia, Ukraine). We
187 used a multivariate linear mixed model to fit the reduction in transmissibility compared to

baseline, as a function of the reduction in mobility indicator compared to baseline, in each country, at each day. The multivariate model corrects for the correlations between the different mobility indicators. The model includes mobility as a fixed effet, and region as a random effect affecting both the intercept and the slope of the relation. Interestingly, we found a correlation between transmissibility and all indicators, and particularly mobility in transit stations (public transport hubs such as subway, bus, and train stations). The model had a coefficient of determination of 93%. A reduction in the mobility in transit stations compared to baseline approximately translated in the same reduction in transmissibility (Table 1). This correlation was found in the whole dataset, in the subset of European countries, and in the subset of USA states.

Dataset / model	**Grocery / pharmacy**	**Parks**	**Transit stations**	**Retail & recreation**	**Residential**	**Workplaces**
full	-0.06 [-0.27 ; 0.15]	**-0.14** [-0.17 ; -0.1]	**1.02** [0.82 ; 1.21]	0.13 [-0.08 ; 0.34]	-0.26 [-0.46 ; -0.06]	-0.02 [-0.15 ; 0.11]
USA states	-0.27 [-0.39 ; -0.15]	**-0.2** [-0.25 ; -0.15]	**1.31** [0.95 ; 1.64]	0.17 [-0.12 ; 0.44]	0.02 [-0.51 ; 0.53]	-0.26 [-0.52 ; 0.02]
Europe	0.33 [-0.03 ; 0.63]	**-0.12** [-0.16 ; -0.09]	**1.02** [0.8 ; 1.24]	-0.14 [-0.43 ; 0.16]	-0.1 [-0.34 ; 0.15]	0.36 [0.2 ; 0.53]

Table 1: Regression coefficients fo the temporal relationship between transmissibility and each of the mobility indicators, in the full dataset, the USA states, and European countries. 95% confidence intervals indicated in parenthesis. Consistent and significant effects are highlighted.

Relationship between probability of detection and intensity of testing:

We last relate the time-varying probability of detection to the intensity of testing. First, we correlate the probability of detection (as of May 8th) with the number of tests performed by inhabitants *across regions*. We did so for 62 regions where test data were available. There was a strong correlation between probability of detection and number of tests per inhabitants (regression coefficient $\beta = 161$ per daily test per inhabitant, $p = 4.0e\text{-}5$) (Fig. 5B).

Second, to examine further how the changing number of tests affects the probability of detection *within a region and across time*, we formulated a simple model of symptom-based testing. The goal of this model is to relate within a region the number of tests conducted on a given day (called T_t) with the inferred probability of detection on that day (c_t). We assume that in the period when the incidence of infections is much higher than the number of tests, the decision to test individuals for SARS-CoV-2 is made on the basis of a set of symptoms. We do not consider contact tracing, as during that period and in the countries examined the number of

infected individuals was too large for this intervention to be practically implemented. The set of symptoms defines a score. SARS-CoV-2 infected and uninfected individuals present two distinct distributions of this score, such that the probability that the individual is truly infected with SARS-CoV-2 increases with this score. Tests are prioritised on individuals with the highest score. This model thus reproduces the fact that the fraction of positive tests increases when tests are more limited compared to the number of infected individuals. For simplicity, we additionally assume that the score in infected and uninfected individuals follows exponential distributions with two distinct rates. Under this model, the probability of detection is given by the solution c_t of:

$$T_t = P_t\, c_t + N\, c_t^{\gamma}$$

(Material and Methods). In this equation, the variable T_t is the total number of tests conducted at day *t*. P_t and N are the number of SARS-CoV-2 infected and non-infected individuals seeking care at day *t*, and who could potentially be tested if the number of tests available allows. P_t is the time-delayed number of infected individuals given by $P_t = \sum_{\tau=0}^{\infty} y(\tau)\, I(t,\tau)$ where $y(\tau)$ is the probability that an individual is detected τ days after infection (when it is detected), while N is assumed to be constant over the considered period. The parameter $\gamma > 1$ describes the distribution of the symptom score in infected individuals relative to that in uninfected individuals. There is no closed form solution for the general solution c_t, but when the distribution of the score is dominated by negative individuals, the probability of detection is approximately a root function of the number of tests:

$$c_t = \left(\frac{T_t}{N}\right)^{1/\gamma}$$

The probability of detection should thus generally increase sublinearly with the number of tests since $\gamma > 1$, and at best, should be proportional to the number of tests (when $\gamma = 1$). This is because tests are prioritised on individuals that are more likely to be infected; as the number of tests increases, the probability of positivity decreases. We also predict that in general, when the number of infected is large, the probability of detection decreases with the number of infected individuals (Material and Methods).

Both predictions were verified in data (Fig. 5). We inferred for each region the best-fitting pair of parameters (N, γ) to relate the inferred probability of detection c_t to the number of tests T_t, using both the approximated and the general model. We found that $\gamma > 1$ for most regions, implying a sublinear relationship as predicted (Fig. 5C). The general model where the

247 probability of detection decreased with the number of testable infected individuals was a better
248 fit only when the attack rate was high, for example in New York state (Fig. 5D, Supplementary
249 Fig. 8).

250 Discussion

251 We developed a discrete time renewal equation model to describe the dynamics of SARS-CoV-
252 2 infections. We fitted this model to the daily cases and deaths in a large number of countries
253 and states (together representing more than four billions individuals), with the following
254 results:

255 (i) Transmissibility declined in all 79 regions examined. The best-fit decline in
256 transmissibility was often smooth, with the decline in transmissibility predating the date
257 of the lockdown. This could be due to non-pharmaceutical interventions implemented
258 before the full lockdown or other behavioural changes. However, the decline in
259 transmissibility as of May 8th was not enough to contain the epidemic in a number of
260 regions.
261 (ii) The probability of case detection increased, was on average 29% across regions as of
262 May 8th, and very rarely above 50%.
263 (iii) Epidemic control was achieved mainly through reductions in transmissibility brought
264 about by social distancing. Case detection and isolation had a limited impact (Fig. 4B),
265 even under the conservative assumption that case detection is followed by perfect
266 isolation. Only a small proportion of cases are detected and about half of the
267 transmission happens before symptom onset. We emphasise that in this period most
268 testing was based on symptoms and not on past contacts with infected individuals. The
269 build-up of immunity in infected individuals also had a very limited impact because the
270 fraction of individuals infected remains small in all regions. Social distancing in the
271 regions considered (totalling more than 4 billions inhabitants) avoided almost 10
272 millions deaths from the beginning of the epidemic to May 8th.
273 (iv) Transmissibility correlated with mobility indicators, and most notably with the
274 presence of individuals in transit stations, both in Europe and in the USA.
275 (v) The inferred probability of detection correlated with the number of tests per capita
276 across regions. However, increasing the number of tests does not proportionally
277 increase the probability of detection. This is explained by the fact that tests are
278 prioritised on individuals most likely to be infected.

Our model and inference rely on several assumptions. First of all, we describe transmission dynamics within a simplified model that does not take into account age structure or household structure. These forms of structure may be weak enough that they can be neglected when describing the overall epidemic trajectory (20). Second, to infer jointly the time-varying transmissibility and probability of detection within a dynamical model, we assumed the temporal change took specific sigmoid functional forms. This differs from other approaches which estimate daily transmissibility as the incidence at a given day divided by past incidence weighted by the distribution of the generation time (21,22). These alternative approaches are more flexible in that they can infer any pattern of time-varying transmissibility. However, they cannot account exactly for the delay in case reporting, and can be very sensitive to noise in the data (21). Fitting a dynamical model with imposed functional forms for transmissibility and probability of detection reduces the sensitivity of inference to noise in the data. Third, and most importantly, inference relies on daily deaths and cases. Deaths are assumed to be perfectly reported. Cases are assumed to be partially reported with a time-varying detection probability. The inferred absolute value of the probability of detection of course strongly relies on the assumed IFR at around 1% on average (and tuned to the specific age structure of each region considered). The approach was validated in a number of regions where systematic test or seroprevalence surveys were conducted (Fig. 1). It is possible that in some of the other regions examined the number of deaths was greatly under-reported, in which case the true number of infected would be much higher than predicted, and the probability of case detection much smaller. However this should not affect the temporal trends in transmissibility or probability of detection, provided that under-reporting is constant in time. Other emerging seroprevalence surveys will give more information on the IFR (or death under-reporting) across regions, but it is notable that the early estimate of IFR in mainland China (8) already allow good predictions (Fig. 1). Lastly, our framework does not take into account the possibility that the IFR changes in time. Such temporal variation in IFR could be caused by overwhelmed health systems (increasing IFR) of better social distancing in at-risk groups (decreasing IFR).

Our method has several advantages. The discrete-time renewal equation makes the minimal assumptions that the transmissibility of an infected individual depends on the age of infection. It allows arbitrary distributions of the generation time, and arbitrary delays between infection and case detection, and infection and death. The distributions of these delays determines the dynamics of the changes in number of cases and deaths following a change in transmissibility. Parameters can be inferred using multiple time series, improving the precision of inference.

312 The daily cases, although dependent on the number of tests available, give an earlier signal of
313 changes in transmissibility than the daily deaths, and suffer less from stochastic effects. The
314 method allows different transmissibility for detected cases (here assumed to be zero, i.e. perfect
315 isolation after detection). This is particularly relevant for accurate inference of transmissibility,
316 as non-pharmaceutical interventions shorten the serial interval (fig. 4A) (17). Lastly, the
317 framework quantifies the immunity acquired by infected individuals.

318 The probability of detection as a function of time in different countries was computed by
319 different means in another study (23). Their statistical approach was based on estimating the
320 case fatality ratio (CFR) adjusted for the delay between infection and deaths, and comparing
321 with the baseline infected fatality ratio estimated in other studies that account for under-
322 reporting (assumed to be 1.4% in their case). Their statistical method allows inferring arbitrary
323 temporal variations in the probability of detection. However, it does not explicitly model the
324 dynamics of transmission. It is unclear how the changing age-of-infection structure of the
325 population upon reductions in transmission will affect the relationship between daily number
326 of deaths and past number of cases, hence the inferred probability of detection, in their
327 approach.

328 We found that tests based on symptoms detected only a small proportion of cases. Our model,
329 importantly, applies in settings where the number of tests is much smaller than the number of
330 individuals presenting to health systems with symptoms suggestive of SARS-CoV-2 infections.
331 Increasing the number of tests does not proportionally increase the proportion of detected
332 individuals. As a consequence of the typically small probability of detection, together with the
333 fact that around half of the transmission is pre-symptomatic, tests followed by isolation of
334 positive cases had very little impact on transmission, and are not sufficient by themselves to
335 control an epidemic with a basic reproductive number of 3 or more. Tracing and testing the
336 contacts of positive cases—a strategy that is not described by our model—identifies a pool of
337 individuals with a 5-10% chance of being positive, up to 10-15% for household contacts
338 (16,24,25). Identification of positive cases through widescale contact-tracing could thus
339 modify the relationship between probability of detection and number of tests and in particular
340 make it more linear. Furthermore, these contacts are isolated earlier than those identified
341 through symptom-based testing (5,26). For these two reasons, contact-tracing and testing is a
342 more efficient way to control the epidemic than symptom-based testing. Thus, if the capacity
343 to trace contacts is limited, the epidemic may be out control as soon as the daily incidence is
344 too large to trace a good fraction of contacts. This pleads for the use of digitical contact tracing

345 apps and/or rapid implementation of additionnal social distancing measures when incidence
346 increases.

347 Lastly, the inferred time-varying transmissibility correlated with mobility indicators (19,27).
348 More precisely, within a multivariate framework we found that the mobility in transit stations
349 was the most highly correlated with transmissibility, a pattern consistent in European countries
350 and the USA (Table 1), and with a regression coefficient close to 1 (a given reduction in
351 mobility corresponds to an equivalent reduction in transmission). The mobility in transit
352 stations could be a general indicator of economic / social activity resulting in more
353 transmission. Public transports could also be a common context of transmission. In support of
354 our finding, individual use of public transport in Maryland was strongly associated with SARS-
355 CoV-2 positivity (28).

356 In conclusion, we developed a framework to estimate time-varying transmissibility and
357 probability of detection from daily cases and deaths in a large number of countries and regions.
358 In the first few months of 2020, control of the epidemic was achieved mostly by reductions in
359 transmissibility, which avoided 10 millions deaths in these 79 regions (representing more than
360 half of the world's population), while case detection and isolation comparatively had a much
361 smaller effect.

362

363 **Methods:**

364 Deterministic transmission dynamics:

365 To model transmission dynamics, we use a discretised version of the renewal equation (e.g.
366 (11)). We follow the dynamics of the number of individuals infected at day *t* who were infected
367 τ days ago, and have not yet been detected and isolated, called $I(t,\tau)$. The transmission
368 dynamics are given by the system of recurrence equations:

369 $$I(t+1,0) = R_{0,t}\,(1 - I_t^{tot}/S_0)\sum_{\tau=0}^{\infty} w(\tau)\, I(t,\tau) \qquad (1a)$$

370 $$I(t+1,\ \tau) = I(t,\ \tau-1)\big(1 - c_t\, y(\tau-1)\big)\ \forall\, \tau \geq 1 \qquad (1b)$$

371 The first equation represents transmission to new susceptible individuals giving rise to infected
372 individuals with age of infection 0. The parameter $R_{0,t}$ reflects transmissibility, and is the basic
373 reproduction number (in the absence of interventions, and when the population is fully
374 suscpetibe, i.e. $I_t^{tot} = 0$). The factor $w(\tau)$ is the fraction of transmission that occurs at age of
375 infection τ, where $\sum_{\tau=0}^{\infty} w(\tau) = 1$. Thus $w(\tau)$ represents the distribution of the generation time
376 of the virus. The infectiousness profile of the virus is linked with the generation time
377 distribution through $\beta(\tau) = R_{0,t}\, w(\tau)$. Transmission is reduced by a factor $1 - I_t^{tot}/S_0$ by
378 population immunity, where S_0 is the initial number of susceptible individuals in the region,
379 assumed to be the total population size. The variable $I_t^{tot} = \sum_{i=1}^{t} I(i,0)$ is the total number of
380 individuals already infected and assumed to be fully immune at time t. The instantaenous
381 reproduction number that accounts for population immunity but not for case isolation is $R_t =$
382 $R_{0,t}\,(1 - I_t^{tot}/S_0)$.

383 The second equation (1b) represents the dynamics of individuals infected in the past.
384 Individuals infected $\tau - 1$ days ago are now of age of infection τ, provided they were not
385 detected and isolated. An infected individual is detected with time-varying probability c_t, and
386 the probability that an individual is detected at age τ (when it is detected) is given by $y(\tau)$,
387 with $\sum_{\tau=1}^{\infty} y(\tau) = 1$. An individual who is detected is removed from the pool of individuals
388 that contribute to further transmission of the disease. The total number of cases detected at day
389 t is thus:

390 $$C(t) = c_t \sum_{\tau=0}^{\infty} y(\tau)\, I(t,\tau) \qquad (2)$$

391 And the number of detected individuals who were infected τ days ago changes as:

392 $$C(t+1,0) = 0 \text{ (when } \tau = 0) \qquad (3a)$$

$$C(t+1,\tau) = C(t,\tau-1) + c_t\, I(t,\tau-1)\, y(\tau-1) \;\; \forall\, \tau \geq 1 \qquad (3b)$$

The total number of infected individuals, be they undetected or detected, that we may call $A(t,\tau) = I(t,\tau) + C(t,\tau)$, follows the equations:

$$A(t+1,0) = R_{0,t}\,(1 - I_t^{tot}/S_0) \sum_{\tau=0}^{\infty} w(\tau)\, I(t,\tau) \qquad (4a)$$

$$A(t+1,\tau) = A(t,\tau-1) \qquad (4b)$$

The fact that incidence (in the first equation) only depends on undetected cases $I(t,\tau)$ emerges from the assumption that detected individuals $C(t,\tau)$ do not transmit.

While in the absence of testing and isolation, the infectiousness profile is given by $\beta(\tau) = R_{0,t}\, w(\tau)$ (with $R_{0,t} = \sum_{\tau=0}^{\infty} \beta(\tau)$), detection and isolation truncates the infectiousness profile at the time of detection t_d (Fig. 4A) with probability $c_t\, y(t_d)$ where t_d is the time of detection. In other words, the effective infectiousness profile is the mixture distribution:

$$\beta_E(\tau) = (1 - c_t)\, R_{0,t}\, w(\tau) + c_t\, R_{0,t} \sum_{t_d=0}^{\infty} y(t_d)\, w(\tau)\, \mathbb{I}_{\tau \leq t_d} \qquad (5)$$

where $\mathbb{I}_{\tau \leq t_d}$ is an indicator variable equal to 1 when $\tau \leq t_d$, and 0 otherwise.

<u>Probability of dying and time to death given infection:</u>

The probability that an infected individual dies is the Infected Fatality Ratio (IFR) denoted *d*, assumed to be constant over time. The probability of dying τ days after infection, given that one dies, is given by $x(\tau)$. The mean number of deceased individuals at day *t* is then given by:

$$D(t) = d \sum_{\tau=0}^{\infty} x(\tau) \left(I(t,\tau) + C(t,\tau) \right) \qquad (6)$$

As death typically occurs at a time when the infected individual does not transmit any longer, and the probability of dying is small (of the order of 1%), we neglect the impact of death on transmission.

<u>Effects of detection and isolation, change in transmissibility and immunity on transmission</u>

We call "effective reproduction number" $R_{0,t}^E$ the instantaneous reproduction number taking into account immunity and case isolation is given by (see also (29)):

$$R_{0,t}^E = \sum_{\tau=0}^{\infty} \beta_E(\tau) = R_{0,t} \left[\underbrace{(1 - c_t)}_{\text{undetected}} + c_t \underbrace{\sum_{t_d=0}^{\infty} y(t_d) \sum_{\tau=0}^{t_d} w(\tau)}_{\text{detected at time } t_d} \right] \qquad (7a)$$

For example, an individual detected at day 0 only infects $R_{0,t}\, w(0)$ individuals on average. Equation (6a) can be rewritten as:

$$R_{0,t}^{E} = \sum_{\tau=0}^{\infty} \beta_E(\tau) = R_{0,t}\left[1 - c_t \sum_{t_d=0}^{\infty} y(t_d)\left(\sum_{\tau=t_d+1}^{\infty} w(\tau)\right)\right] \quad (7b)$$

Thus, the effective reproduction number $R_{t_{final}}^{E}$ on the 8th of May (t_{final}), including the impacts of detection and isolation and immunity may be written as the product of the initial basic reproduction number, times three factors that all reduce transmission:

$$R_{t_{final}}^{E} = R_{0,t_{init}} \underbrace{\left(1 - \mathcal{A}_{t_{final}}\right)}_{\text{(i) immunity}} \underbrace{\left(1 - \mathcal{B}_{t_{final}}\right)}_{\text{(ii) reduced transmissibility}} \underbrace{\left(1 - \mathcal{C}_{t_{final}}\right)}_{\text{(iii) detection and isolation}} \quad (8)$$

With $\mathcal{A}_{t_{final}} = I_{t_{final}}^{tot}/S_0$, $\mathcal{B}_{t_{final}} = 1 - R_{0,t_{final}}/R_{0,t_{init}}$, and

$\mathcal{C}_{t_{final}} = c_{t_{final}} \sum_{t_d=0}^{\infty} y(t_d)\left(\sum_{\tau=t_d+1}^{\infty} w(\tau)\right)$.

<u>Parameter estimates</u>

We fix the distributions of the generation time $w(\tau)$, the distribution of time from infection to death $x(\tau)$, the distribution from infection to detection $y(\tau)$, and the infection fatality ratio d to values estimated previously.

Parameter	**Symbol**	**Value**	**Reference**
Distribution of generation time	$w(\tau)$	Log-normal(1.77, 0.888) Mean 7 days SD 4.5 days	(9,16,30)
Distribution of time from infection to symptom onset	-	Log-normal(1.518, 0.472)	(13)
Distribution of time from infection to death	$x(\tau)$	Calculated by convoluting distribution from infection to onset and from onset to death. The latter is Gamma(5, 0.25)	(9)
Distribution of time from infection to detection	$y(\tau)$	Calculated by convoluting distribution from infection to onset and from onset to detection	(13)
Infection fatality ratio	d	Depends on the age structure of the country, around 1% on average	(8)
Probability of detection	c_t	Inferred	-
Transmissibility	$R_{0,t}$	Inferred	-

Table 2: Summary of model parameters

Generation time

We assume the generation time is lognormally distributed with mean 7 days and standard deviation 4.5 days (9) (Supplementary Fig. 4). This is the generation time when the infected individual is not tested. A positive test is assumed to be followed by perfect isolation of the infected individual and interruption of transmission. This effectively truncates the distribution

437 of generation time (Fig. 4A). Two factors make estimation of this generation time difficult:
438 first, the generation time, the time from an infection to another infection, is often approximated
439 by the serial interval, the time between symptom onset in an infector and symptom onset in the
440 infectee. These two quantities have the same mean, but the variance of the generation time
441 should in general be smaller than that of the serial interval (31). Second, measuring the serial
442 interval requires to identify infectees and their infectors. The fact that the infector needs to be
443 identified could bias the serial interval towards lower values. For example, in a large study in
444 the Shenzhen province in China, the serial interval had mean 6.3 days overall and 8.1 days if
445 the infector was isolated more than two days after infection (16). Thus, in settings where most
446 infections are undocumented, the typical serial interval (and generation time) may be longer
447 than that estimated in other work (e.g. mean 5 days in (5)), motivating the mean of 7 days
448 chosen here.

449 Note that the chosen serial interval distribution affects the absolute value of the basic
450 reproduction number, but does not affect either the inferred temporal trend in basic
451 reproduction number or the absolute value of the probability of detection.

452 *Time from infection to detection*

453 The time from symptom onset to case detection was inferred from published data on 150 cases
454 from various countries (13). We used the time between the midpoint date of symptom onset
455 and the midpoint date of case detection. We excluded 31 cases for which the date of case
456 detection was not available or there was very large uncertainty on the date of symptom onset.
457 We inferred that the time from symptom onset to detection was gamma-distributed with mean
458 2.2 days [95% CI 1.6-3.2] and SD 2.7 days [2.0-3.8] (shape 0.69 [0.55-0.82] and rate 3.2 [2.5,
459 4.5]). The fit of a Weibull distribution was comparable to that of the gamma (Supplementary
460 Fig. 5).

461 The distribution of time from infection to detection was computed from the convolution of the
462 distribution of time from infection to symptom onset (13), and our inferred distribution of time
463 from symptom onset to case detection, assuming independence of the two times. The
464 distribution of time from infection to symptom onset has mean 5 to 6 days (Supplementary Fig.
465 6).

466 *Time from infection to death*

467 The distribution of the time from infection to death was estimated using data from 41 patients
468 in Wuhan analysed elsewhere (12). The time from symptom onset to death was gamma-

469 distributed with a mean of 20 days and a standard deviation of 10 days. This estimate is close
470 to that of other studies (24 deceased cases from mainland China, mean and SD of time from
471 onset to deaths 18.8 / 8.5 days (8); 34 deceased cases from mainland China, mean and SD 20.2
472 /11.6 days (32).

473 *Infection fatality ratio*

474 For each region studied, we computed an overall infection fatality ratio that takes into account
475 the age pyramid of the country. To this end, we used the infection fatality ratio (IFR) estimated
476 in nine age classes, [0, 9], [10, 19], etc., [80+] in mainland China (8). Other estimates similarly
477 stratified by age, for mainland China and for France, are very similar (Supplementary Fig. 1).
478 The IFR climbs from close to 0% in 0 to 39 years old, up to 5 to 10% in individuals aged 80
479 years old or more.

480 Likelihood method:

481 To fit the model and infer transmission and case detection parameters, we use data on the
482 number of confirmed cases over time and the number of deaths over time in 79 states and
483 countries from different public sources detailed below. We include all states and countries that
484 had a daily incidence of 10 deaths or more at least once as of 23th April. As we want to estimate
485 the impact of sudden social distancing measures in an essentially uncontrolled epidemic, we
486 exclude South Korea and Japan from the analysis. In these two countries, SARS-CoV-2 was
487 introduced earlier and strong control measures including social distancing and contact tracing
488 were immediately in place.

489 Simulating the deterministic model gives the expected number of detected cases $C(t)$ and
490 deaths $D(t)$ at time t as a function of model parameters. We assume that the probability to
491 observe a certain number of cases (resp. deaths) in the data at day t is the density of a negative
492 binomial distribution with mean given by the theoretical predictions for cases (resp. deaths),
493 and dispersion parameters that we infer. The overall likelihood is the product of these
494 probabilities over all days. For the number of deaths, we include the period from the first day
495 to the last day when at least 1 death and 5 cases were recorded. For the number of cases, we
496 include the period from the first day to the last day when at least 5 cases were recorded.

497 We mainly estimate the time-changing transmissibility $R_{0,t}$ and the time-changing probability
498 of detection c_t.

For the time-changing transmissibility, we fit two functional forms. First we assume that $R_{0,t}$ is a step function with a sharp transition from a high pre-control value to a low post-control value, at a fixed date $t_{control}$ corresponding to the date of implementation of the control measure:

$$R_{0,t} = R_{0,pre} \text{ if } t < t_{control} \qquad (9a)$$

$$R_{0,t} = R_{0,post} \text{ if } t \geq t_{control} \qquad (9b)$$

For the sharp change in transmissibility, we infer the two values $R_{0,pre}$ and $R_{0,post}$. Furthermore, to investigate the possibility that transmissibility changed in a more gradual way, we assume $R_{0,t}$ is a smooth declining sigmoid function:

$$R_{0,t} = R_{0,pre} + \frac{R_{0,post} - R_{0,pre}}{1 + e^{-k_R(t - t_R)}} \qquad (10)$$

Where $R_{0,pre}$ is the basic reproductive number before social distancing measures, $R_{0,post}$ is the basic reproductive number after social distancing, k_R is the steepness of the logistic curve, and t_R is the time when the basic reproductive number is intermediate between $R_{0,pre}$ and $R_{0,post}$. The step function is a special case of the logistic when k is large and $t_R = t_{lockdown}$. For the smooth change in transmissibility, we infer the two values $R_{0,pre}$ and $R_{0,post}$, the steepness k_R and the time t_R.

For the time-changing detection probability, we assume an increasing logistic function:

$$c_t = c_{min} + \frac{c_{max} - c_{min}}{1 + e^{-k_C(t - t_C)}} \qquad (11)$$

We infer the four parameters c_{min}, c_{max}, k_C and t_C. Note that we constrain the parameter c_{min}, the initial probability of detection, to be small, in [0.0001, 0.001]. We fit three models: (i) a model based on death data only with the step function of transmissibility, (ii) a model based on death and case data with the step transmissibility function; and (iii) a model based on death and case data with the smooth transmissibility function. These three models are fitted by maximum likelihood. We first find an optimal likelihood value by 50 iterations of the Nelder-Mead algorithm starting from different initial parameters. We then run a Markov chain Monte Carlo (MCMC) sampling of the likelihood function with bounded parameters (equivalent to uniform priors for all parameters in a Bayesian framework). We let the chain run for 10^6 steps and record the parameter values from 2×10^5 to 10^6 steps. This sample is used both for maximum likelihood parameters (if a better parameter set is found than with the Nelder-Mead algorithm) and for confidence intervals.

Symptom-based test model

The model

We relate the fraction of infected individuals detected to the number of daily RT-PCR tests performed and the incidence of infection. Each day, the testable individuals seeking care are composed of two populations:

- SARS-CoV-2 infected individuals. The number of such individuals is time-varying and is denoted by $P_t = \sum_{\tau=0}^{\infty} y(\tau)\, I(t,\tau)$ where $y(\tau)$ is the probability that an individual is detected at age of infection τ (given that it is detected) (Fig. 5A).

- Non-SARS-CoV-2 infected individuals. The number of such individuals is assumed to be constant and is denoted by N. We acknowledge that a more complete model would allow for this number to vary in time, for example to account for seasonal infections by respiratory diseases like influenza or seasonal coronavirus that may contribute to the pool of testable individuals.

We assume that contexts in which we apply our model are characterized by a number of tests smaller than the number of testable individuals, $T_t < P_t + N$ where T_t is the number of tests available at time *t*. Thus the T_t tests are prioritised on the subset of individuals most likely to be infected by SARS-CoV-2. Individuals presenting to health centers with symptoms suggestive of SARS-CoV-2 are characterised by a score such that the probability of SARS-COV-2 infection increases with the score. Given the limited number of tests available each day, a threshold score is defined and tests are performed only for patients above this score. Formally, denoting by $\phi_{P_t}(s)$ and $\phi_N(s)$ the distribution of the score *s* in infected and uninfected individuals, the (time-varying) threshold score s_{max} is the solution of:

$$T_t = \int_{s_{max}}^{+\infty} \left[\phi_{P_t}(s) P_t + \phi_N(s) N\right] ds \qquad (12)$$

In the absence of detailed information on the choice of individuals to test in different regions at different stages of the pandemic, we further assume for simplicity that the scores are distributed exponentially. We set the rate of the exponential distribution ϕ_{P_t} to 1 without loss of generality, and we denote $\gamma > 1$ the rate of ϕ_N:

$$\phi_{P_t}(s) = e^{-s} \qquad (13a)$$

$$\phi_N(s) = \gamma e^{-\gamma s} \qquad (13b)$$

The fact that $\gamma > 1$ guarantees that the probability that an individual is positive increases with the score. Plugging the distributions (13) in the implicit formula to define the threshold score s_{max} (12) yields:

$$T_t = P_t\, e^{-s_{max}} + N\, e^{-\gamma\, s_{max}} \qquad (14)$$

The probability of detection c_t, defined as the ratio between positive tests results and the number of testable infected individuals P_t, is the area of the ϕ_{P_t} distribution above the threshold s_{max}:

$$c_t = \frac{1}{P_t}\int_{s_{max}}^{\infty} \phi_{P_t}(s) P_t\, ds = e^{-s_{max}} \qquad (15)$$

Replacing with equation (15) in equation (14), we find that c_t is the solution of:

$$T_t = c_t\, P_t + c_t^{\gamma}\, N \qquad (16)$$

This generally defines an implicit function $c_t(T_t, P_t)$ of the number of testable infected at day t, P_t and the number of available tests T_t. We can simplify this general solution in two ways. First, in the limit when the number of infected P_t is much smaller than the number of uninfected N, and γ is not too large, the probability of detection is:

$$c_t \approx \left(\frac{T_t}{N}\right)^{\frac{1}{\gamma}} \qquad (17a)$$

That is, the probability of detection increases as a root function of the normalised number of tests. In general, when the number of testable infected individuals P_t is not negligible, the solution c_t of equation (16) decreases with P_t. When the number of testable infected individuals P_t is small, the solution (17a) can be better approximated by:

$$c_t \approx \left(\frac{T_t}{N}\right)^{\frac{1}{\gamma}} - P_t \frac{1}{\gamma\, T_t} \left(\frac{T_t}{N}\right)^{\frac{2}{\gamma}} \qquad (17b)$$

In this approximation the probability of detection decreases linearly with the number of infected P_t.

Parameter inference

We verify the model predictions using the inferred probability of detection c_t together with data on the daily number of tests T_t, and the number of testable infected individuals P_t inferred from the dynamical model in different regions. We used the *nls* method from the *stats* package in the software R (33).

First, we use the general solution of equation (16). This solution is a non-linear function $c_t(T_t, P_t)$ with parameters N and γ. We infer the parameters N and γ by minimizing the mean square error between the inferred c_t and the prediction. In most cases (except, notably New York and New Jersey states) the coefficient of determination was as good with the simplification of the model where c_t is approximated as a root function of T_t only (equation(17a)) (Supplementary Fig. 8). The general solution improved the fit all the more than the the attack rate was larger, as predicted by the model (Supplementary Fig. 8).

Data sources

Epidemiological data:

For France, we used data from OpenCOVID19 available at https://github.com/opencovid19-fr/data. This website curates data from *Agence nationale de santé publique*, the French governmental public health agency.

For Italy, we used data from the Civil Protection Department (Dipartimento della Protezione Civile), available at https://github.com/pcm-dpc/COVID-19. This data includes daily cases and deaths, and daily number of tests.

For other European countries, we used data from the European Center for Disease Control (ECDC) available at https://opendata.ecdc.europa.eu/covid19/casedistribution/

For American states, we used data from the COVID Tracking Project that compiles data from American official sources, available at https://covidtracking.com/api/v1/states/daily.csv . This data includes daily cases and deaths, and daily number of tests.

For other countries, we used data from the Center for Systems Science and Engineering (CSSE) at Johns Hopkins University (JHU), available at https://github.com/CSSEGISandData/COVID-19

Daily number of tests data for regions other than Italy and American state were compiled from Our World in Data at https://covid.ourworldindata.org/data/owid-covid-data.csv

We considered test data only for regions for which the number of tests was strictly superior to the number of cases recorded for at least 80% of the days. The reported number of tests are sometimes exactly equal to the number of cases that day, indicating that negative tests are not reported. Since we ignore whether negative tests are not reported or reported at a later date (as sometimes suggeted by a peak in the number of reported tests a few days after), we exclude these datapoints and exclude regions where this artefact is often observed.

Age structure data:

We collected data on the number of individuals in age categories 0-9, 10-19, …, 80+, for different states and countries, from the following sources:

Region	Source	Web address (accessed 04/09/2020)
USA	US Census bureau	https://population.un.org/wpp/Download/Files/1_Indicators%20(Standard)/EXCEL_FILES/1_Population/WPP2019_POP_F07_1_POPULATION_BY_AGE_BOTH_SEXES.xlsx
Quebec	Canadian government	https://stat.gouv.qc.ca/statistiques/population-demographie/structure/population-quebec-age-sexe.html#tri_pop=10
British Columbia	Canadian government	https://www12.statcan.gc.ca/census-recensement/2016/dp-pd/prof/details/page.cfm?Lang=E&Geo1=PR&Code1=59&Geo2=PR&Code2=01&SearchText=Canada&SearchType=Begins&SearchPR=01&B1=All&type=0
Ontario	Canadian government	https://www12.statcan.gc.ca/census-recensement/2016/dp-pd/prof/details/page.cfm?Lang=E&Geo1=PR&Code1=35&Geo2=PR&Code2=01&Data=Count&SearchText=35&SearchType=Begins&SearchPR=01&B1=All&Custom=&TABID=3
Hubei province, China	China National Bureau of Statistics	https://www.citypopulation.de/en/china/admin/42__hubei/
All others	United Nations	https://population.un.org/wpp/Download/Files/1_Indicators%20(Standard)/EXCEL_FILES/1_Population/WPP2019_POP_F07_1_POPULATION_BY_AGE_BOTH_SEXES.xlsx accessed

Mobility data:

We used Google mobility data available at https://www.google.com/covid19/mobility/

Data availability:

Code and data is available on https://github.com/FrancoisBlanquart/covid_model

Acknowledgements:

We thank Florence Débarre for helpful comments. We thank the many people involved in the collection and curation of the epidemiological data that we use. F.B. was supported by a Momentum grant from the CNRS. A.B was supported by a scholarship from Ecole Polytechnique.

Competing interests:

None.

632 **Bibliography**

633 1. Rambaut A. Phylodynamic Analysis| 176 genomes| 6 Mar 2020. Virol Httpvirological
634 Orgtphylodynamic-Anal-176-Genomes-6-Mar-2020356 Accessed. 2020;15.

635 2. Li Q, Guan X, Wu P, Wang X, Zhou L, Tong Y, et al. Early Transmission Dynamics in
636 Wuhan, China, of Novel Coronavirus–Infected Pneumonia. N Engl J Med. 2020 Mar
637 26;382(13):1199–207.

638 3. Kucharski AJ, Russell TW, Diamond C, Liu Y, Edmunds J, Funk S, et al. Early
639 dynamics of transmission and control of COVID-19: a mathematical modelling study.
640 Lancet Infect Dis. 2020 May 1;20(5):553–8.

641 4. Riou J, Althaus CL. Pattern of early human-to-human transmission of Wuhan 2019
642 novel coronavirus (2019-nCoV), December 2019 to January 2020. Eurosurveillance
643 [Internet]. 2020 Jan 30 [cited 2020 Jul 28];25(4). Available from:
644 https://www.eurosurveillance.org/content/10.2807/1560-7917.ES.2020.25.4.2000058

645 5. Ferretti L, Wymant C, Kendall M, Zhao L, Nurtay A, Abeler-Dörner L, et al.
646 Quantifying SARS-CoV-2 transmission suggests epidemic control with digital contact
647 tracing. Science [Internet]. 2020 May 8 [cited 2020 Jun 24];368(6491). Available from:
648 https://science.sciencemag.org/content/368/6491/eabb6936

649 6. Casey M, Griffin J, McAloon CG, Byrne AW, Madden JM, McEvoy D, et al. Pre-
650 symptomatic transmission of SARS-CoV-2 infection: a secondary analysis using
651 published data. medRxiv. 2020 Jun 11;2020.05.08.20094870.

652 7. Salje H, Kiem CT, Lefrancq N, Courtejoie N, Bosetti P, Paireau J, et al. Estimating the
653 burden of SARS-CoV-2 in France. Science [Internet]. 2020 May 13 [cited 2020 Jun 24];
654 Available from:
655 https://science.sciencemag.org/content/early/2020/05/12/science.abc3517

656 8. Verity R, Okell LC, Dorigatti I, Winskill P, Whittaker C, Imai N, et al. Estimates of the
657 severity of coronavirus disease 2019: a model-based analysis. Lancet Infect Dis
658 [Internet]. 2020 Mar 30 [cited 2020 Apr 7];0(0). Available from:
659 https://www.thelancet.com/journals/laninf/article/PIIS1473-3099(20)30243-7/abstract

660 9. Wu JT, Leung K, Bushman M, Kishore N, Niehus R, de Salazar PM, et al. Estimating
661 clinical severity of COVID-19 from the transmission dynamics in Wuhan, China. Nat
662 Med. 2020 Apr;26(4):506–10.

663 10. Hauser A, Counotte MJ, Margossian CC, Konstantinoudis G, Low N, Althaus CL, et al.
664 Estimation of SARS-CoV-2 mortality during the early stages of an epidemic: a
665 modeling study in Hubei, China, and six regions in Europe. medRxiv. 2020 Jul
666 12;2020.03.04.20031104.

667 11. Flaxman S, Mishra S, Gandy A, Unwin HJT, Mellan TA, Coupland H, et al. Estimating
668 the effects of non-pharmaceutical interventions on COVID-19 in Europe. Nature. 2020
669 Jun 8;1–8.

12. Wu JT, Leung K, Bushman M, Kishore N, Niehus R, Salazar PM de, et al. Estimating clinical severity of COVID-19 from the transmission dynamics in Wuhan, China. Nat Med. 2020 Mar 19;1–5.

13. Lauer SA, Grantz KH, Bi Q, Jones FK, Zheng Q, Meredith HR, et al. The Incubation Period of Coronavirus Disease 2019 (COVID-19) From Publicly Reported Confirmed Cases: Estimation and Application. Ann Intern Med. 2020 Mar 10;172(9):577–82.

14. Long Q-X, Liu B-Z, Deng H-J, Wu G-C, Deng K, Chen Y-K, et al. Antibody responses to SARS-CoV-2 in patients with COVID-19. Nat Med. 2020 Jun;26(6):845–8.

15. Kucirka LM, Lauer SA, Laeyendecker O, Boon D, Lessler J. Variation in False-Negative Rate of Reverse Transcriptase Polymerase Chain Reaction–Based SARS-CoV-2 Tests by Time Since Exposure. Ann Intern Med [Internet]. 2020 May 13 [cited 2020 Jun 24]; Available from: https://www.acpjournals.org/doi/10.7326/M20-1495

16. Bi Q, Wu Y, Mei S, Ye C, Zou X, Zhang Z, et al. Epidemiology and transmission of COVID-19 in 391 cases and 1286 of their close contacts in Shenzhen, China: a retrospective cohort study. Lancet Infect Dis [Internet]. 2020 Apr 27 [cited 2020 Jun 24]; Available from: http://www.sciencedirect.com/science/article/pii/S1473309920302875

17. Ali ST, Wang L, Lau EHY, Xu X-K, Du Z, Wu Y, et al. Serial interval of SARS-CoV-2 was shortened over time by nonpharmaceutical interventions. Science [Internet]. 2020 Jul 21 [cited 2020 Jul 31]; Available from: https://science.sciencemag.org/content/early/2020/07/20/science.abc9004

18. Unwin HJT, Mishra S, Bradley VC, Gandy A, Vollmer M, Mellan T, et al. State-level tracking of COVID-19 in the United States. 2020 May 20 [cited 2020 Jun 26]; Available from: https://openreview.net/forum?id=NuBVOoSnlTh&noteId=wcYAXeS-Why

19. Miller AC, Foti NJ, Lewnard JA, Jewell NP, Guestrin C, Fox EB. Mobility trends provide a leading indicator of changes in SARS-CoV-2 transmission. medRxiv. 2020 May 11;2020.05.07.20094441.

20. Pellis L, Cauchemez S, Ferguson NM, Fraser C. Systematic selection between age and household structure for models aimed at emerging epidemic predictions. Nat Commun. 2020 Feb 14;11(1):906.

21. Gostic KM, McGough L, Baskerville E, Abbott S, Joshi K, Tedijanto C, et al. Practical considerations for measuring the effective reproductive number, Rt. medRxiv. 2020 Jun 23;2020.06.18.20134858.

22. Cori A, Ferguson NM, Fraser C, Cauchemez S. A New Framework and Software to Estimate Time-Varying Reproduction Numbers During Epidemics. Am J Epidemiol. 2013 Nov 1;178(9):1505–12.

23. Russell TW, Golding N, Hellewell J, Abbott S, Pearson CAB, van Zandvoort K, et al. Reconstructing the global dynamics of unreported COVID-19 cases and infections | CMMID Repository [Internet]. [cited 2020 Jul 31]. Available from: https://cmmid.github.io/topics/covid19/Under-Reporting.html

24. Jing Q-L, Liu M-J, Yuan J, Zhang Z-B, Zhang A-R, Dean NE, et al. Household Secondary Attack Rate of COVID-19 and Associated Determinants. medRxiv. 2020 Apr 15;2020.04.11.20056010.

25. Li W, Zhang B, Lu J, Liu S, Chang Z, Peng C, et al. Characteristics of Household Transmission of COVID-19. Clin Infect Dis [Internet]. [cited 2020 Jul 31]; Available from: https://academic.oup.com/cid/article/doi/10.1093/cid/ciaa450/5821281

26. Hellewell J, Abbott S, Gimma A, Bosse NI, Jarvis CI, Russell TW, et al. Feasibility of controlling COVID-19 outbreaks by isolation of cases and contacts. Lancet Glob Health. 2020 Apr 1;8(4):e488–96.

27. Nouvellet P, Bhatia S, Cori A, Ainslie K, Baguelin M, Bhatt S, et al. Report 26: Reduction in mobility and COVID-19 transmission.

28. Clipman SJ, Wesolowski AP, Gibson DG, Agarwal S, Lambrou AS, Kirk GD, et al. Rapid real-time tracking of non-pharmaceutical interventions and their association with SARS-CoV-2 positivity: The COVID-19 Pandemic Pulse Study. Clin Infect Dis [Internet]. [cited 2020 Sep 5]; Available from: https://academic.oup.com/cid/advance-article/doi/10.1093/cid/ciaa1313/5900759

29. Grassly NC, Pons-Salort M, Parker EPK, White PJ, Ferguson NM, Ainslie K, et al. Comparison of molecular testing strategies for COVID-19 control: a mathematical modelling study. Lancet Infect Dis [Internet]. 2020 Aug 18 [cited 2020 Aug 27]; Available from: http://www.sciencedirect.com/science/article/pii/S1473309920306307

30. Ma S, Zhang J, Zeng M, Yun Q, Guo W, Zheng Y, et al. Epidemiological parameters of coronavirus disease 2019: a pooled analysis of publicly reported individual data of 1155 cases from seven countries. medRxiv. 2020 Mar 24;2020.03.21.20040329.

31. Britton T, Scalia Tomba G. Estimation in emerging epidemics: biases and remedies. J R Soc Interface [Internet]. 2019 Jan [cited 2020 Jul 21];16(150). Available from: https://www.ncbi.nlm.nih.gov/pmc/articles/PMC6364646/

32. Linton NM, Kobayashi T, Yang Y, Hayashi K, Akhmetzhanov AR, Jung S, et al. Incubation Period and Other Epidemiological Characteristics of 2019 Novel Coronavirus Infections with Right Truncation: A Statistical Analysis of Publicly Available Case Data. J Clin Med. 2020 Feb;9(2):538.

33. R Core Team. R: A Language and Environment for Statistical Computing. Vienna, Austria: R Foundation for Statistical Computing; 2018.

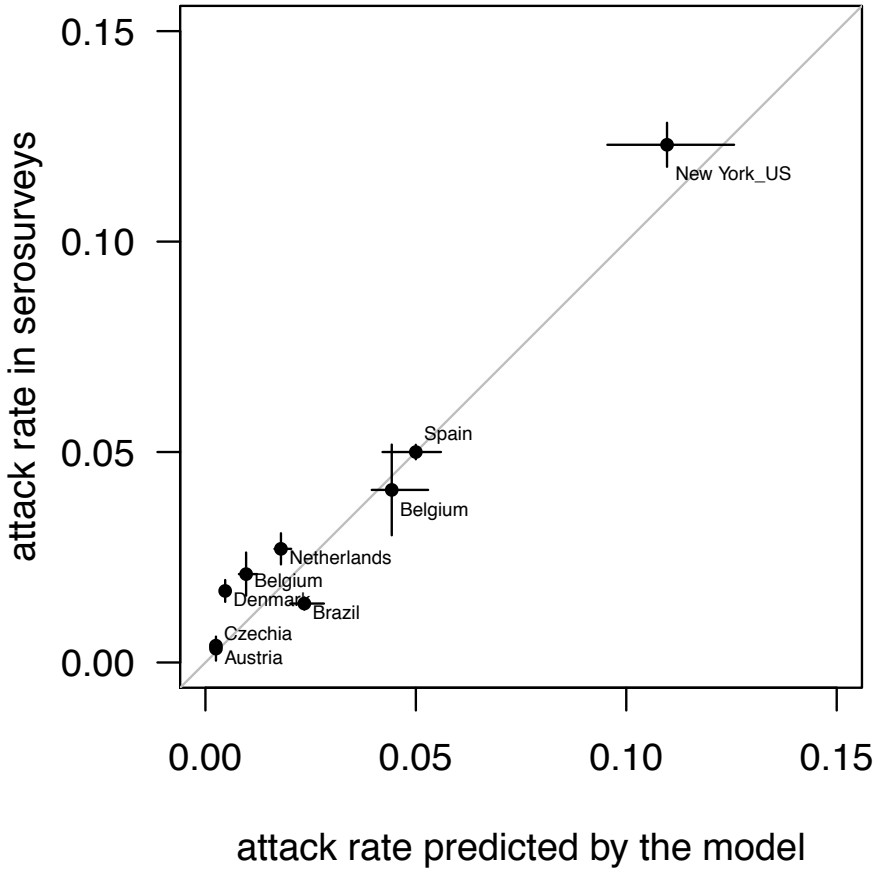

Figure 1: Comparison of the total number of infected (attack rate) found in systematic serological test surveys with that predicted by our model. The segments are 95% confidence intervals (for the data, binomial confidence intervals; for the model, estimated from the MCMC sample). We used the model with the smooth sigmoid reduction in transmission; the model with the sharp transition gave very similar results.

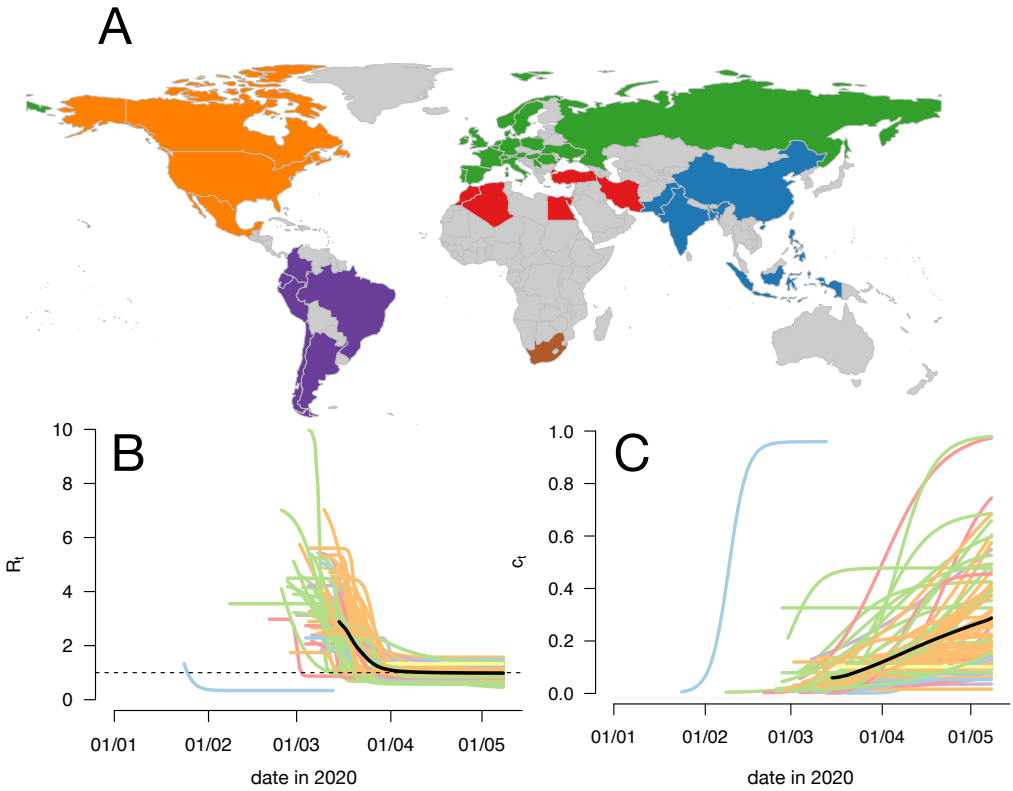

Figure 2: **Panel A** shows the map of the regions considered in this study, colored by geographic areas (Europe+Russia, North Africa/Middle East, Asia, South Africa, Central-South America, North America). The USA are represented by 33 states. China is represented by the Hubei province. **Panels B, C** show the inferred transmissibility and the probability of detection as a function of time for all regions. The overall mean is a thick black line. The early blue trajectory is that of the Hubei province in China.

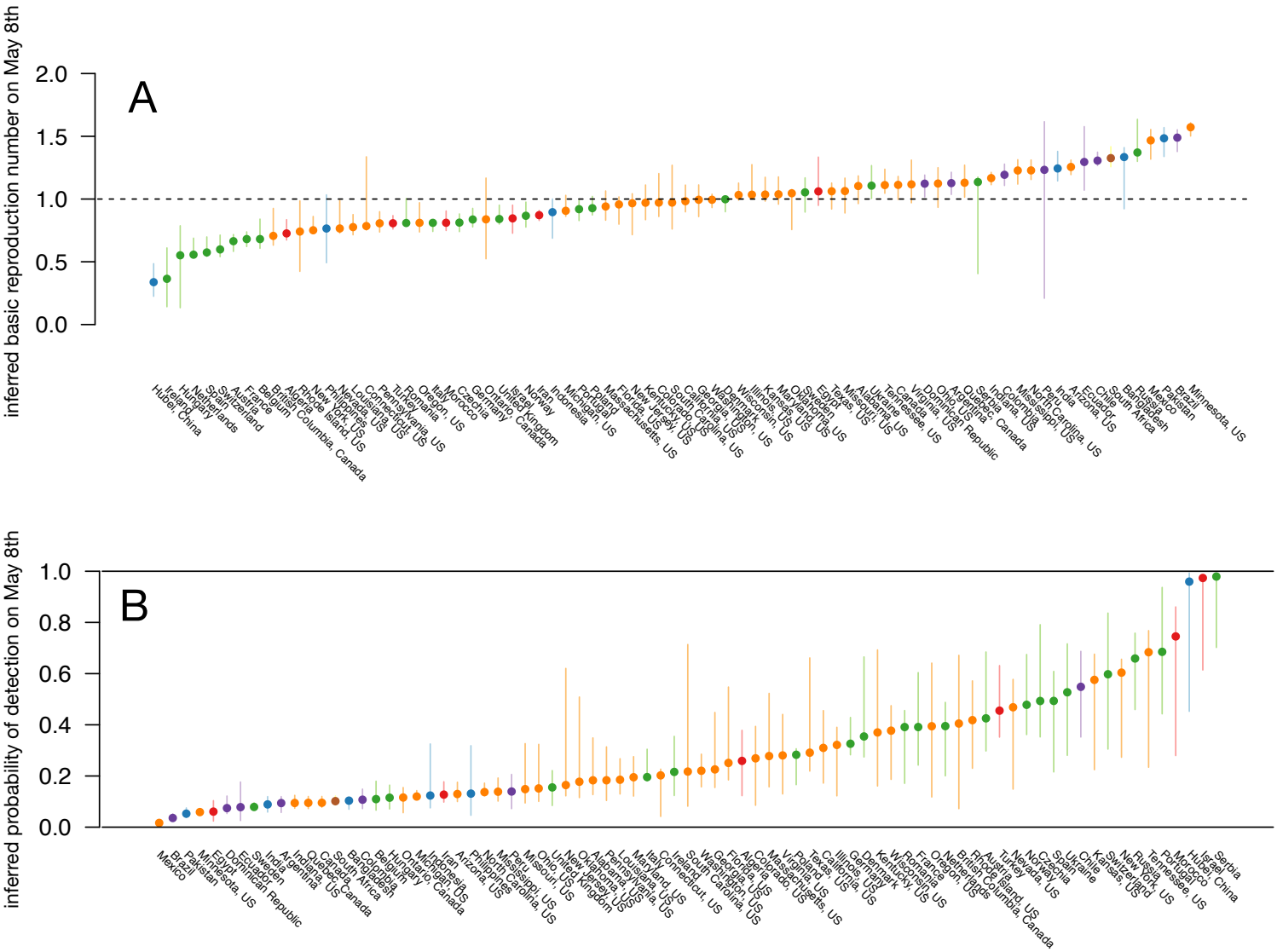

Figure 3: Inferred transmissibility R_t (**panel A**) and probability of detection c_t (**panel B**) as of May 8th, for each region. The point is the maximum likelihood estimate and the segment shows the 95% confidence intervals.

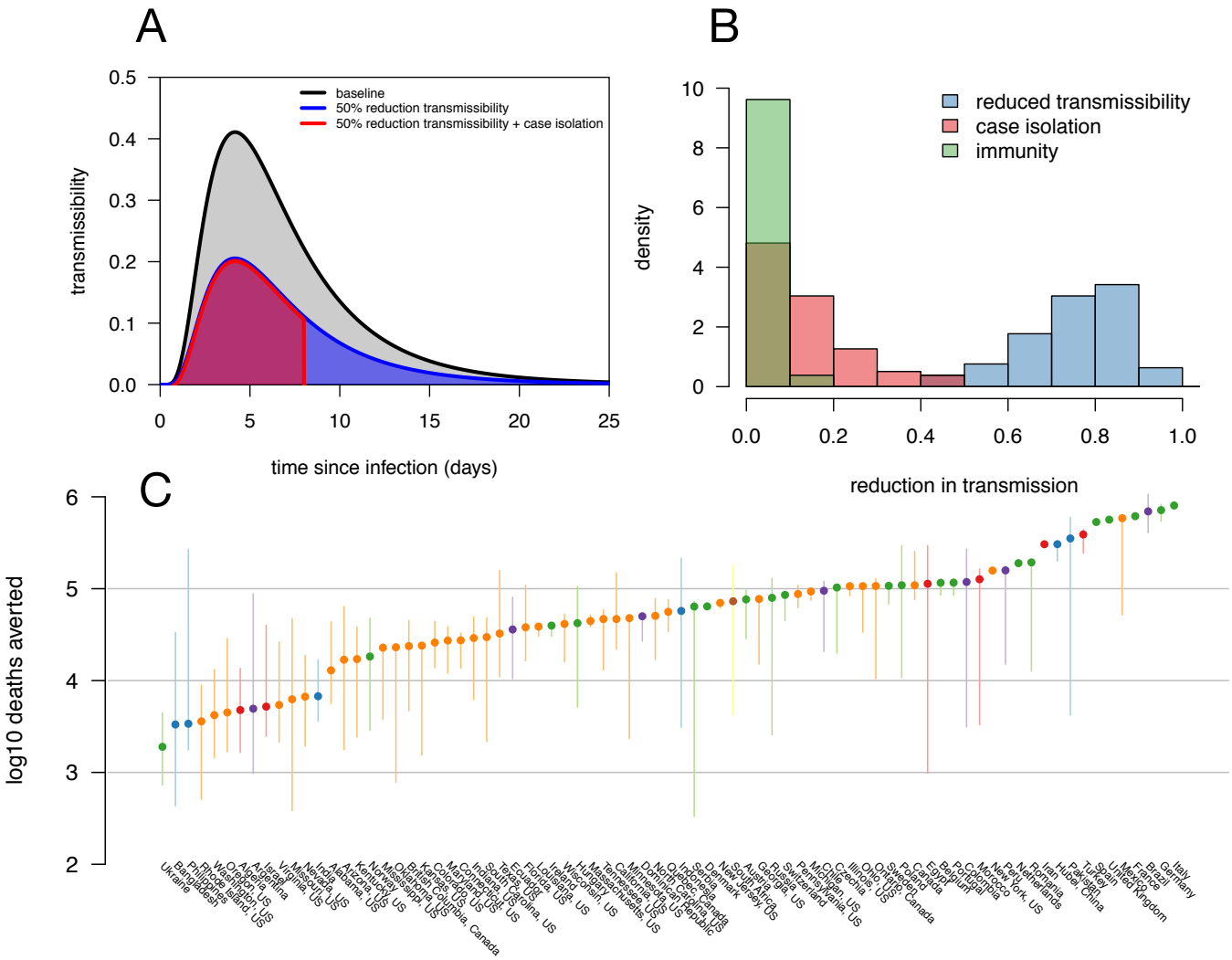

Figure 4: **Impact of control measures and immunity on transmission dynamics. Panel A** illustrates how social distancing and case isolation reduce transmission of the disease. The basic reproduction number is given by the area under the curve. A reduction in transmissibility uniformly reduces the R_t (blue curve and area), while detection and case isolation truncates the serial interval (red curve). **Panel B** represents the distribution of the reduction in transmission caused by social distancing (blue), detection and isolation (red) and immunity of already infected individuals (green) across the 79 regions. **Panel C** represents the $\log_{10}$ number of deaths averted by social distancing between the beginning of the epidemic and the 8th May 2020.

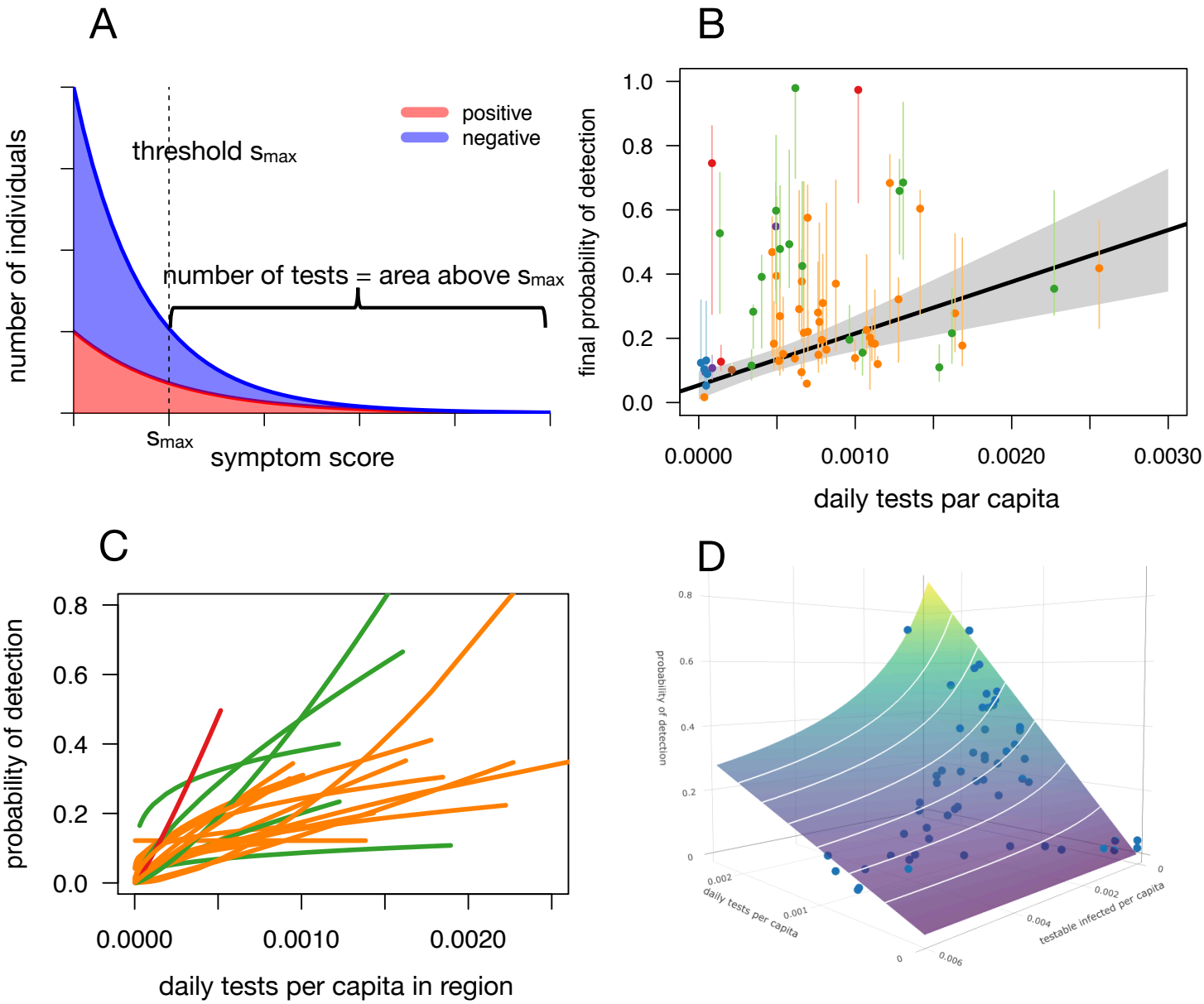

Figure 5: **Relationship between probability of detection and number of tests. Panel A** shows stacked distributions of the disease score for positive (red) and negative (blue) individuals. The fraction of positive individuals increases with the score. The number of tests performed is the area to the right of the threshold (vertical line). **Panel B** represents the final probability of detection as a function of number of daily tests per capita (over the 7 days preceding 8th May) for the 62 regions with available test data. **Panel C** shows the predicted root-function relationship between proportion of detected and daily tests for the 33 regions with sufficient available test data. **Panel D** shows the proportion of detected a function of daily tests and the number of testable infected presenting for a test, for the New York state (one of the high-prevalence states where the proportion detected declines with the number of infected as predicted at high prevalence).